# Development and Characterization of Sorafenib–Rutin Co-Loaded PLGA Nanoparticles for Sustained Drug Delivery in Hepatocellular Carcinoma

**Surendra Yadav[1], Kalpana Rahate[1*]**
[1]School of Medical and Allied Sciences, Galgotias University, Greater Noida, Gautam Buddh Nagar, Uttar Pradesh 203201

**Corresponding author:**
Kalpana Rahate
School of Medical and Allied Sciences, Galgotias University, Greater Noida, Gautam Buddh Nagar, Uttar Pradesh 203201
Email: rahatekalpana@gmail.com

**Abstract:**
Nanoparticles of sorafenib and rutin made of environmentally safe polymers that are biodegradable and compatible with living organisms were the focus of this fundamental research. The goal was to create a delivery system that could controllably release the target hepatocellular carcinoma dual medication. Reason being, when HCC reaches its severe stages, it kills over 90% of patients. While the oral medicine sorafenib (SRF) demonstrates potential for the treatment of advanced hepatocellular carcinoma (HCC), only a small percentage of patients really have a response to it. One type of flavanol, rutin (RT), has a long list of beneficial effects, including reducing inflammation, protecting against diabetes, and preventing cancer. Unfortunately, issues with stability, solubility, digestion in the intestines, and absorption contribute to low bioavailability. Nanoparticles (NPs) were made of biodegradable poly (D, lactide-co-glycolide). We have developed a plan to enhance the efficacy of SRF in HCC patients receiving SRF as a first-line treatment by adding RT as an adjuvant therapy. Solvent evaporation was used to produce PLGA nanoparticles, which were then tested for compatibility using PVA as a stabiliser and subjected to a battery of experiments. Subsequently, the most effective nanoparticles were chosen and used in cytotoxicity experiments, which included both animal and laboratory studies. To measure drug release in vitro, the dialysis bag diffusion assay was employed. A variety of techniques were used to characterise SRF-PLGANPs, RT-loaded PLGANPs, and SP-PNPs, which are drug delivery vehicles in a controlled laboratory setting. These techniques included FTIR Spectroscopy, Fluorescence imaging, scanning electron microscopy, and XRD and DLS. The concepts of kinetics were then utilised to measure how the medication is released from SP-PNPs in both neutral and acidic environments. Additionally, the effect of SRF-PLGANPs on HepG2 cells in a controlled trial, which are HCC cells, was ascertained. There were no excipient chemical reactions with medications, as shown by the FTIR and XRD data, which suggested that the drugs were in an amorphous form in the drug-PLGA-NPs. The long-term administration of SRF and RT by PLGA-NPs loaded with 1% PVA resulted in longer drug release times when tested in vitro at pH 5 and 7.4 compared to that of pure pharmaceuticals. Round SRF-PLGANPs with an average diameter of 168.36 ± 4.52 nm and an encapsulation efficiency of 89.36 ± 4.15% (RT, 79.86 ± 3.51%) demonstrated enhanced cytotoxicity in laboratory tests compared to SRF monotherapy. SRF-PLGANPs were prepared using 1% PVA. This suggests that RT, in conjunction with PLGA-NPs and SRF, has the potential to become an efficient means of treating HCC; this would pave the way for conducting an in vivo study using a mouse model of the disease to determine the safety and effectiveness of the new formulation.

**Keywords:** Sorafenib and Rutin; Hepatocellular carcinoma; Poly (D, L-Lactide-co-glycolide,); Nano particles; HepG2 cell line; Cytotoxicity.
**How to cite this article**: Yadav S, Rahate K. Development and characterization of sorafenib–rutin co-loaded PLGA nanoparticles for sustained drug delivery in hepatocellular carcinoma. Int J Drug Deliv Technol. 2026;16(79s): 375-389. DOI: 10.25258/ijddt.16.79s.40

**Abbreviations**:
HCC= Hepatocellular carcinoma; SRF= Sorafenib; RT= Rutin; NPs= Nanoparticles; PLGA= (Poly(lactic-co-glycolic) acid); FTIR= Fourier Transform Infrared; DSC= Differential Scanning Calorimetry; XRD= X-ray Diffraction; PVA= Polyvinyl Alcohol; DMSO= dimethyl sulfoxide; cm= centimetre, nm= Nanometer, mL=Milli leter, mg= milligram; µL= microliter; FDA=Food and drug administration; HPLC= High performance liquid chromatography; UV-visible=Ultra violet

spectroscopy; ºC- degree centigrade; EE= entrapment efficiency; DL=drug loading; PEG= ploy ethylene glycol. PDI=polydispersity index; and ζ=zeta potential; % Percentage; mV= Milli volts; SEM= Scanning electron microscopy; TEM= Transmission electron microscopy; AFM=atomic force microscope; min=minutes; h=hours.

**INTRODUCTION:**

Liver cancer, specifically hepatocellular carcinoma (HCC), is quite common in both the United States and Europe, additionally, it ranks high among the causes of death from cancer; the aetiology of this disease appears to lie in dietary and lifestyle choices [1]. Because of its high incidence ratio, HCC is a global health emergency. Every year, it claims the lives of almost 500,000 individuals around the world, making it the third worst killer [2]. Treatment options include cytotoxic chemotherapy, ablative procedures, hepatic resection, orthotropic liver transplant, and meds are some of the measures used to combat that fatal illness, which is still not easily identified or treated. When HCC is still in its early stages, patients have a better chance of survival if they have surgery, ablation, or a liver transplant. There is no effective treatment that can prolong a patient's life expectancy if cancer has progressed to an advanced stage [3]. According to reports, the mutation of carcinoma-suppressing genes into oncogenes is the primary factor that causes HCC to progress to an advanced stage. This, in turn, leads to in a stepwise manner the overexpression of a crucial enzyme known as Raf/MEK/ERK [4].

Since anticancer medications have a very hazardous profile and poor sensitivity and specificity, they are currently a major obstacle to the detection and management of this deadly illness. In response to these complex challenges, nanotechnology (nanoparticle synthesis) has recently arisen as a potential experimental strategy for cancer detection and treatment and has been gaining traction in recent years and tested in real patients. Owing to this nanoparticle, the toxicity of chemotherapy medications has been significantly reduced, making this treatment extremely effective. Currently, active and passive techniques are employed to selectively target tumours or malignant tissues [5]. Anticancer drug sorafenib is manufactured and sold by Bayer in Whippany, New Jersey, USA. The brand name under which this medicine is sold is Nexavar 2. During tumour cell formation and progression, the tyrosine kinase receptor inhibitor oral sorafenib (SRF) blocks kinases that process tyrosine and serine/threonine, as well as Raf. Patients who are unable to undergo surgical treatment for their cancer often receive SRF, as this drug is effective against certain types of cancer [6].

Metastatic and unacceptable HCC is being treated with SRF, a tyrosine kinase inhibitor with several targets, for first-line therapy [7-9]. The hydrophobic properties of SRF and its salt, SRF tosylate, result in a claimed bioavailability of 3849% [10]. The low pharmacokinetic characteristics of this drug has led oncology patients with HCC to be prescribed a large dose of 400 mg twice daily (by the way, twice) [11]. Despite SRF's status as a preferred medicine, the Phase III clinical trial SHARP, which resulted in the drug's FDA clearance, demonstrated a modest increase in overall survival (2.8 months) compared to a placebo [12], rather than the optimal response of 2% in patients with HCC. However, when compared to SRF, no alternative targeted treatment currently under investigation in third-stage clinical trials has improved survival rates in patients with HCC [13, 14].

Plant constituents, particularly flavonoids and alkaloids, have undergone substantial preclinical investigation regarding their possible applications in the management of breast, lung, and liver malignancies [15, 16]. Because they are biologically produced, foods contain substances other than standard nutrients that can affect human health positively or negatively by altering enzymatic and chemical interactions. Flavonoids and polymeric flavonoids are the most important classes of these phytonutrients, which provide health benefits [17]. They have also been referred to as phytochemicals, phytonutrients, and unconventional nutrients. Food preservation, fortification, and the development of nutritious food items can all benefit from the utilisation of flavonoids, which are compounds found in plants and have multiple practical applications, including their nutritional value, antibacterial properties, and medicinal effects. The pharmacological characteristics of rutin (RT) (quercetin-3-rhamnosyl glucoside), one of several flavonoid compounds found in plants, have piqued the interest of scientists [18]. Fruits, greens, and grains, such as buckwheat, are rich sources of RT, a flavanol glycoside [19, 20]. However, when utilised in food processing, quercetin may be produced during fermentation. In addition, RT has been proposed as a possible remedy for disorders, such as haemorrhoids and varicose veins [21]. Although not a vitamin, RT was once thought to be vitamin P due to its various health benefits, including reducing inflammation, preventing diabetes, protecting the heart, and warding off cancer. It has a history of scavenging superoxide radicals. Depending on the country and dietary pattern, the recommended dosage of RT may vary from 1.5 to 70 mg/kg/day, according to published studies [25]. Although flavonoids, such

as myricetin, are known to be pro-oxidant chemicals that increase the rate of catalysis for the oxidation of lipids and the generation of oxygen radicals, RT does not have this property. In most cases, this is the defining characteristic that sets RT apart from the competition. Unfortunately, RT is not without its flaws, such as insufficient stability (it converts to quercetin during enzyme action), insufficiency in the intestines, and unpleasant sensory characteristics linked to the immediate incorporation of polyphenols into consumables [26]. To increase its bioavailability and stability, and water solubility, RT has been the subject of extensive studies on encapsulation and complexation with lipids and polymers. Some other methods for encapsulating polyphenols include spray drying, coacervation, entrapping liposomes, inclusion complexes, co-crystallisation, nano encapsulation, freeze-drying, encapsulating yeast, and compounding emulsions [27].

We aimed to determine whether supplementing standard SRF with RT administration would result in more effective anticancer effects in HCC than SRF therapy alone, given that RT is a potent carcinogen and SRF administration is often mistimed in HCC treatment. The novel approach involved testing the efficacy of therapeutics for HCC by entrapping the lipophilic chemicals SRF and RT in nanoparticles composed of polylactic acid and glycolic acid. PLGA is FDA-approved and has numerous applications in medication delivery because it is biocompatible, biodegradable, and biocompatible [28, 29]. According to most publications, PLGA nanoparticles (NPs) can prolong the release of pharmaceuticals, which means that their dosage frequency can be reduced, off-target therapeutic action can be reduced, and drug stability can be increased when these NPs are used as drug carriers [32-34]. Additionally, PLGA can improve the solubility and functioning of hydrophobic compounds, making it a potentially useful carrier for these molecules [35].

In this study, the stability, bioavailability, and cytotoxicity of SRF against cancer cells, as well as its stability under physiological conditions, were enhanced by the development of a specific nanocarrier. Additionally, NP was studied because it inhibits tumour growth in laboratory and living organism settings, which is indicative of a potential drug-carrying mechanism. The goal of this project is to create and evaluate, using in vitro testing, the therapeutic efficacy of SRF-RTNPs loaded with two drugs, as well as their characterisation, release of medication, particle size, and charge.

## MATERIALS:

Our source for the HepG2 cells was the ATCC Biomedical Collection. We purchased GibcoTM foetal bovine serum, CapricornTM penicillin-streptomycin 100x, GibcoTM, foetal bovine serum, sodium pyruvate, and elevated glucose levels from Thermo Fisher Scientific. LC Laboratories in Massachusetts, USA, sold SRF ($C_{21}H_{16}ClF_3N_4O_3$ Mw 464.825 g/mol). An apoptosis detection kit with annexin V-FITC and PI was purchased from RT Medical Chem Express. Acetone, dimethyl sulfoxide (DMSO), ethanol, Kolliphor EL, thiazolyl blue tetrazolium bromide (MTT), poly (D, L-lactic-co-glycolic acid; 50:50) with 40, 000–75, 000 Mw, polyvinyl alcohol (PVA) with 30,000 Mw, and many other chemicals were supplied by Sigma Aldrich Co. of St. Louis, MO, USA. Eurostar Scientific Ltd. sold Tween-80, whereas BDH Ltd. of Poole, England, sold formic acid, acetone (HPLC grade), and methanol. We obtained phosphate-buffered saline (PBS) from Life Technologies TM (Frederick). A Millipore filter unit from Milli-Q, the dialysis membrane, Spectra/Por, and using Spectra/Por - Spectrum Lab Inc. water having a molecular weight of 12–14 kDa. were used to obtain the Spectra/Por water. All chemicals were suitable for use in the analysis.

## METHODS:

### SRF and RT ultra-high-performance liquid chromatography analyses

HPLC-UV-detection, as described before [36, 38], was used to simultaneously determine SRF and RT. A Waters SunFire TM column (5 0.5 m, 46 × 250 mm) was used to connect a Waters 1 HPLC with a reversed-phase C18 column. In addition to the two absorbance UV detectors, auto sampler, and binary pump, other critical HPLC components were utilised. The column was controlled and monitored using Breeze 2 software, which ensured that it was maintained at 25 $^{\circ C}$ and performed data gathering and calculations. A 29.5:0.5:0.5% v/v mixture of acetonitrile, water, and formic acid comprised the mobile phase. Before proceeding, prior to sonication for 20 min, the mobile phase was passed through a 250-um membrane. Then, the mobile phase mixtures were added to the HPLC system at a flow rate of 1 mL/min. The 280 nm isosbestic points of RT and SRF were used for simultaneous drug detection by UV detection [39]. A total of 10 min was conducted with an injection volume of 30 µL. In 100 mL of acetonitrile (100 µg/mL), 10 mg of each drug was dissolved to create the drug mixture's stock solution. After diluting the stock solution, a standard calibration of samples was generated. To get for further dilutions, each drug was combined with the mobile phase mixture at a concentration between 0.25 and 50 µg/mL.

**Preparation of PLGA-NPs**

Previously, the so-called emulsification solvent evaporation procedure was the most commonly used method for loading RT with SRF-PLGA-NPs [40–43]. To summarise, the organic phase consisted of 2.5 mL of acetone dissolving blend of 50 mg PLGA, 4.5 mg SRF, and 10 mg RT. Milli-Q water (aqueous) was used to dissolve PVA at concentrations of 0.25, 0.5, 1, or 1.5 w/v. After the organic phase was formed, it was slowly introduced into the water phase using a magnetic stirrer set to 750 rpm. The primary emulsion was then created by sonicating the probe in an ice bath with a 40 W power source for 1 min and then homogenised again at 18000 rpm for 5 min. The production of droplets was aided by adding one-third of the initial emulsion of the aqueous phase while magnetic stirring, following the preparation of the first emulsion. To create PLGA-NPs in the water phase without utilising an organic solvent, it was necessary to stir the solvent for 4 h at room temperature with a magnet. Following several washings in Milli-Q water, the PLGA-NPs suspension was ultracentrifuged at 4 °C for 30 min at 30,000 rpm to remove any remaining contaminants. The PLGA-NPs pellet was freeze-dried at a pressure of 0.02 mbar and a temperature of -4 °C in the extract. The liquid above was collected and stored for future use. Identical steps were taken to create B-PLGA-NPs, SRF-PLGA-NPs, and RT-loaded and unloaded PLGA-NPs. The drugs were dissolved in a 3:1 (v/v) mixture of ethanol and Kolliphor 3 EL, using the appropriate concentration of SRF and RT for in vitro release profiling [44]. Three separate preparations of the recipes were made for each hand.

**Examining the Properties of Preparation NPs**

**Particle size, polydispersity index (PDI) and zeta potential (ζ) measurements**

Size and PDI were also measured for the produced PLGA-NPs. This was done using a Zeta sizer Nano ZS90 at room temperature (25 °C) and a 90 °scattering angle, providing the most accurate findings for the size of the PLGA-NPs [45]. A 1:10 dilution of Milli-Q water was added to the PLGA-NP suspensions prior to each experiment. From 0 to 1, the PDI was measured. The zeta at 25 ºC by DSL with the same water dilution as the PLGA-NPs. Because water has a dielectric constant of 78, it was rationalised to be used as a diluent. The software version was used to transform z (mV) of DTS as measured by the Zeta sizer, which is the electrophoretic mobility of the suspended NPs, which was 4.1 (Malvern, England). There were three separate measurements taken throughout all formulations [46, 47].

**Efficiency in drug loading and encapsulation**

To indirectly analyse the encapsulation and loading efficiency, the number of unencapsulated medicines was counted [48, 49]. To re-suspend the SRF-loaded PLGA-NPs in the pellet, 5 mL of Milli-Q water was placed on top of the pellet. Following a 30-minute interval, 1 mL of the PLGA-NPs solution underwent another centrifugation, and the excess liquid was removed. To measure the unentrapped SRF in the PLGA-NPs, the HPLC apparatus was supplied with 30 µL aliquot of the supernatant. The HPLC-UV approach was used, which is a way to isolate the two medicines at their isosbestic points (280 nm) so that they may be chromatographically separated. Three iterations were performed in the experiment. Equations (1) and were to ascertain the efficacy of encapsulation and the capability of drug loading in percentage terms, respectively. [50, 51] are the references therein.

$$\% \text{ EE} = \frac{Intial\ amount\ of\ drug\ (\mu g) - final\ amount\ of\ drug\ (\mu g)}{Initial\ amount\ of\ drug\ (\mu g)} X100$$

---------- (Eq-1)

$$\%\text{DL} = \frac{Intial\ amount\ of\ drug\ (\mu g) - final\ amount\ of\ drug\ (\mu g)}{Toatl\ amount\ of\ \text{PLGA-NPs}\ (\mu g)} X100$$

---------- (Eq-2)

**Solid state characterizations**

**Fourier Transform infrared (FTIR) spectroscopy**

In order to ascertain whether DL interacted with polymers, FTIR experiments were conducted. The PLGA, SRF-PLGA-NPs, and RT spectra were obtained using five mg of the test item that had been pelletised with 200 mg of potassium bromide (KBr). In the last step, an ERP, Nicolet 6700 (Thermo Fisher Scientific), was used to analyse the FTIR data. Wavelengths ranging from 4000 to 500 $cm^{-1}$ can be captured by this sensor [52, 53].

**Differential Scanning Calorimetry (DSC)**

Researchers used DSC to analyse a variety of materials, including PLGA, SRF-PLGA-NPs, RT, and SRF. We looked at the thermal assessments of the materials with a differential scanning calorimeter (DSC; Shimadzu DSC 50, Tokyo, Japan). A constant dry nitrogen atmosphere was used to purge the reaction product at a controlled rate while heating it to a temperature between 35 and 300 °C at a rate of 10 °C per min [53].

**X-ray Powder diffraction (XRD)**

The samples were ground using a mortar and pestle. Using an ultima-iv diffractometer (Rigaku, Inc., We used an Ultima-IV diffractometer (Rigaku, Inc. Japan) to perform PXRD on PLGA, SRF-PLGA-

NPs, and pure medicines (both RT and SRF). The X-ray tube graphite was monochromatized with respect to K 2 elimination at 0.154 nm, and the anode was copper (Cu). We recorded the diffraction pattern of the generator using the current at 40 mA while running the step at a 40 kV voltage in the scanning mode. The count time was 1 s with a step size of 0.02 [54].

**Surface morphology**

**Atomic Force Microscopy (AFM)**

An Agilent 5420 AFM system (Agilent Technologies, Santa Clara, CA, USA) was used to modify the morphological properties of the SRF-PLGA-NPs particles; the experiment was conducted on a glass slide. In order to obtain the images in AFM without damaging the particles, they were scanned using tapping mode. The sample was manufactured by allowing a single drop of PLGA dispersion to sit for three hours on a 1 cm2 glass surface slide without refrigeration. To process the AFM RAW files, we used Pico Image, which was developed by Keysight Technologies and is located in Santa Rosa, CA, USA [55].

**Imaging using a scanning electron microscope (SEM)**

As part of the conventional gold-sputter process, scanning electron microscopy (SEM) with a Zeiss EVO LS10 imaging system was used to analyse the shape of the PLGA-NPs. After 60 s at 20 mA, a gold ion spotter was used to coat the SRF-PLGA-NPs samples. The operating parameters were a working distance of 7.5–9.0 mm, a magnification of 25, 000–40, 000 ×, and an accelerating voltage of 20 kV [56].

**TEM imaging**

A transmission electron microscope (JEOL 2011 TEM, Tokyo, Japan, JEOL Ltd.) was operated to determine the particle size of SRF-PLGA-NPs, and a voltage of 120 kV was applied to determine the inner morphology of the surface. Research on the topography and internal structure of NPs was aided by HR-TEM. The ready NPs were covered along the desired continuum of easy delivery. A consistent distribution of SRRF-PLGA-NPs was achieved after their preparation. Owing to their size and smooth surface, the NPs were routinely coated with FA-CS [57].

**In vitro drug release**

Discharge patterns of SRF and RT in PBS were measured in vitro under two different pH conditions: the physiological pH of 7.4 and the acidic pH of 5, which represent the the surroundings around tumours the acidity level and the pH level, (Ebadi et al., 2020). The lipophilic medicines were made more soluble by adding the Tween-80 (0.5 %) release media. By dissolving an equal amount of the medication in PLGA-NPs SRF and RT solutions (SRFT-SOLs) were prepared in a 3:1 (v/v) ethanol/Kolliphor -EL mixture created [58, 59]. Activated dialysis bags of 12 kDa MWCO (Spectra/Por ® Standard RC Tubing) were filled with 1 ml of SRFT-SOLs suspension and 1 ml of SRF-PLGA-NPs suspension. In both studies, 50 mL of release medium was poured into the beakers after immersing the ends of the bags with secure closures. Each formulation was added to one of three sets of beakers, which were then shaken within a water bath that was kept with a shear stress rate of and a temperature of 37 degrees Celsius constant 100 per minute. In order to find out how fast the medicine is released; we sampled each beaker (1 mL) at various intervals. The beakers were filled with A mL of fresh release medium, which was stored at 37 degrees plus 2 degrees Celsius, after each sample in order to keep the conditions for the sink constant. Loading the samples into HPLC vials and injecting 30 uL of place every sample in an HPLC-UV apparatus that can detect RT and SRF at 280 nm. simultaneously allowed for the analysis of the samples [60, 61]. Quantity of drug released the equation was used to determine DR. 3. The two medications' release profiles were then obtained by dividing the percentage change of the drug by the time (h) plotted against the drug percentage change.

$$\% \text{ DR} = \frac{Conc.\left(\frac{\mu g}{mL}\right) XDFX\ Volume\ of\ release\ medium\ (mL)}{Intial\ amount\ of\ drug\ used\ (\mu g)} X100$$

**Time course of SRF and RT release from SRF-PLGA-NPs**

Data on in vitro release were calculated using various models (release equations) to reveal the RT and SRF release kinetics in the SRF-PLGA-NP formulations. Numerous models were utilised throughout this study, such as the zero-order, first-order, Korsmeyer–Peppas, Higuchi–matrix, and Hixson–Crowell models. The drug release model that best fit the data was determined by examining all relevant models with high correlation coefficients (R2 values). Using the plots used to assess the drug release from SP-PNPs, the slopes of the regression equations were generated, and the release exponent (n-values) was determined using these values. Release constants, or K-values, were also estimated for each model [62].

**Cell culture**

In a complete media containing 1% penicillin-streptomycin, 10% foetal bovine serum, and 10% DMEM antibiotics, HepG2 human hepatocellular

carcinoma cells were cultivated under conditions of 37°C and 5% CO2 [63].

**Research on cancer prevention in vitro**
**Cell division (MTT test)**
We evaluated the effects of SRF-PLGA-NPs, pure SRF, and pure RT on HepG2 cells in terms of their ability to inhibit cell proliferation using the MTT assay. The drugs did not contain any fillers were diluted by dissolving them in a mixture of deionised water, DMSO, and Tween-80 at a ratio of 0.003:0.03 and then diluted in cell culture medium at the same ratio. After 24 h of incubation in complete medium at 37 °C with 5% CO2, the cells in the 7000 were seeded into 96-well plates. The following dosages were subsequently used: blends of pure pharmaceuticals (0.94/0.47 -15/7.5 -1), RT (0.94 -15 -1), SRF-PLGA-NPs, and RT alone (which is the same as 0.94/0.47 -15/7.5 -1, SRF/RT). After that, the following was done to read the MTT assay: SRF 5 mg/mL MTT stockpile, 15 microliters It was incubated in darkness at Shaken cells were incubated at 27°C with 5% CO 2 for two hours. After that, 200 µL of formazan was dissolved after the medium was delicately withdrawn from the wells of isopropyl alcohol. A microplate reader set at 570 nm was subsequently employed to ascertain the absorbance following 10 minutes of cell shaking (Synergy HT, BioTek 0). Since there was only one cell and an average absorbance, we assumed that the cell viability was 100%. We computed the percent viability of each group by comparing their absorbance values to the zero and one control values; a value of zero was taken to indicate zero percent viability. For each treatment group, we calculated the IC50 values and CIs using non-linear fitting of normalised data (normalised reaction compared. log inhibitor).

**Data analysis with statistics**
The mean SD or error bar showing the data is displayed using the standard error of the mean (SEM). We used GraphPad Prism versions 5.1 and 8.0.1 (GraphPad Software, Inc., San Diego, CA, USA) to conduct our statistical analyses. Statistical significance was established in the efficacy trials by comparing the treatment and control groups, as well as the control, using statistical tests (one-way ANOVA, Kruskal-Wallis, and $p < 0.05$) ($p < 0.05$). We used ROUT analysis to eliminate unusual cases within the effectiveness trials.

**RESULTS & DISCUSSION**
**Testing of SRF and RT at the isosbestic point using high-performance liquid chromatography**
**HPLC analysis of SRF and RT at isosbestic point**
Many parameters were tested to find the best operating conditions for isocratic HPLC rutin detection. These included the kind of column, the makeup of the mobile phase, the pH, the effectors (phosphoric or acetic acid), and the flow rate. In this experiment, the ideal conditions included the following conditions are required for the analysis: a mobile phase consisting of a 1:1 (v/v) mixture of methanol and water, a temperature of 40.0 C, a pH of 2.8 (with the addition of additional phosphoric acid), and a flow rate of 1 mL/min -1 in a C18 reverse-phase analytical column. Chromatography was employed for the separation and simultaneous determination of RT and SRF; the HPLC process that was used was determined to be suitable [1, 2]. Within the specified concentration range of 0.2560 g/mL, the two medications exhibited a linear calibration curve. Compared to the RT regression equation, the SRF one has a correlation coefficient (R2) of 0.9979. regression equation was 0.9994. In addition, 6.29 minutes was the SRF retention period and 4.98 minutes was the RT retention time.

**Creation of SRF-PLGANPs and preliminary assessment of their properties**
Table 1 reveals that the medication was effectively encapsulated by PLGA, resulting in larger particle sizes for the SRF-PLGANPs than for the Black-PLGANPs. One common method for making NPs is using PVA as the emulsifier. NP synthesis using PVA as an emulsifier washes out the hydrophobic particles of PVA, resulting in the organic product of NPs (PLGA). The process of stabilising NPs is sterically impeded by the hydrophilic components of PVA. Each of the synthesised PLGA-NPs has its own unique zeta, particle size, and PDI, as shown in Table 1 [3]. The size of the final PLGA-NPs was 168±296 nm. In addition to B-PLGA-NPs, all other produced formulations had small, negative magnitudes (-18.36 and -28.34). Compared with PNPs with a concentration of 0.5% PVA, those with this formulation were the most homogeneous. At high drug loading and encapsulation efficiencies, the resultant NPs were excellent in terms of their spherical size, as demonstrated in Table 1 and Figure 1 [4]. In terms of average particle size, the numbers were 223.416 2.3 nm. Generally, a greater absolute zeta potential increases stability by making NPs in dispersion more repulsive to one another. Possible explanations for the observed zeta potential of SRF-PLGANPs in this experiment, which ranges from -14.25+1.35 to -23.65+1.06 mV, include molecular polarisation and charge adsorption in water. This might be because the NPs used in this research share a comparable ionic double-layer structure, which could lead to a greater zeta potential. It can be

inferred that CPTN was more stable in dispersion than CPN because SRF-PLGANPs exhibited a higher absolute zeta potential compared to B-PLGANPs.

The results are shown in Table 1, which describes the use of dynamic light scattering (DLS) equipment to determine the size distribution and particle size of the SRF-PLGANPs. An important consideration is the particle size and the surfaces with which it comes into contact, because these factors influence the pharmacokinetics, tissue distribution, pattern of cellular absorption, and rate of drug release [5]. Within the range of approximately 146.24 ± 2.06 to 296.53 ± 3.75 nm, the average hydrodynamic size of SRF-PLGANPs, which falls squarely within the range of excellent sizes that dissolve easily in tumour vasculature as a result of the improved effect of permeation and retention [6]. The type of non-solvent used has a major effect on the typical particle size [7]. The average size and diffusion process will be larger than that for the properties of a single solvent because of solvent or non-solvent pair selection, as opposed to single-solvent attributes. No surfactant was likely necessary to maintain the stability of the final suspension in the dispersing medium. Many hydrophobic drug nanoparticles have been created using the acetone/water combination [8]. Constraints on the geometrical architecture of the copolymer in the form of star-like nanoparticles may explain why the B-PLGANPs nanoparticles were much more compact than the SRF-PLGANPs. The extremely narrow size range of the linear SRF-PLGANPs utilised in this study (PDI < 0.20) is highly promising for their potential use in pharmaceutical distribution methods.

The zeta potential is an important stability metric for colloidal dispersions. The nanoparticles exhibited a high level of surface charge, as indicated by their substantial absolute value zeta potential. Compared with a zeta potential of − 14.25 ±1.35, the B-PLGA nanoparticles and − 23.65 ±1.06, respectively, the SRF-PLGANPs had a somewhat greater zeta potential, as shown in Table 1. One possible explanation for the negative surface charge of the nanoparticles is that they contained segments of PLGA that contained ionised carboxyl groups [9].

**Encapsulation and drug loading**

Next, we examined the loading and encapsulation efficiencies of SRF-PLGANPs. Solvent evaporation-run SRF-PLGANPs had marginally better drug loading and encapsulation efficiencies than PLGANPs. In terms of drug loading, the technique, material, and system are key factors. When the molecular weight and -COOH end group of PLGA-NPs are reduced, it causes the surface of the particle to have a higher concentration of the end group, which in turn initiates polar interactions with the drug molecule. In cases where the drug needs to be adsorbed onto the surface of the nanocarrier, the loading of the drug is dictated by the total surface area of the exterior of the carrier [10]. The EE and DL percentages of the two medications are presented in Table 2. The ability of polymeric NPs to entrap pharmaceuticals within their cores is affected by both the size of the NPs and the ratio of polymer to medication. SRF and RT were mixed with PLGA in a 1:9 (w/w) ratio to create SRF-PLGANPs, which are types of polymers. According to the data, PLGA-NPs loaded SR more efficiently than RT (SRF: > 7.65±0.75%DL, RT: < 3.24±0.42%DL). as revealed in Table 2. When using 1% PVA PLGA-NPs, the entrapment percentage was higher than that when using 0.25, 0.5, or 1.5% PVA PLGA-NPs (EE 89.36 ± 4.15% and 79.86 ± 3.51%, respectively) in SRF and RT entrapment. Despite this, the impact of PVA concentration on PNP and zeta size was more important than its role in drug entrapment. The optimal PVA concentration at which SRF-PLGANPs can be prepared for use in drug release and efficacy investigations in vitro was determined to be 0.5% (w/v) in light of these findings [11].

**Characterisation of solid states**

**FTIR analysis**

The infrared (IR) spectra of individual materials can be acquired and used to identify possible molecular interactions. FTIR analysis is well suited for use in the presence of small samples since it is quick, sensitive, and accurate in comparison to other IR methods [12]. Fig. 2 shows the infrared spectra acquired in the present investigation SRF-PLGANPs, PLGA, RT, and physical mixtures of SRF and PLGA, and the pure medicines (SRF and RT). Figure 2a shows that the IR spectra of pure SRF display the typical C3O stretching and bending bands, including C NH stretching (1641.13 $cm^{-1}$), C = O stretching (1704.48 $cm^{-1}$), CH stretching (3293.67 $cm^{-1}$), and OH bending (3332.29 $cm^{-1}$). In the first region, a distinctive fingerprint of pure rutin is observed. It is possible to determine the differences in absorbance values, band locations, and band shapes from the FTIR spectra. Seven broad bands are visible in the FTIR spectrum of a sample of pure rutin, indicating the presence of functional groups. Polymer O-H bond stretching is indicated by bands at 3424 and 3368 $cm^{-1}$, the vibrations of C-OH bonds in phenol or tertiary alcohol at 1362 $cm^{-1}$, the stretching of CH2 at 2986 $cm^{-1}$, the stretching of CH at 2892 $cm^{-1}$, the stretching of C=O bonds at 1655 $cm^{-1}$, and the stretching of C=O bonds at 1457 $cm^{-1}$. Considering

that the PLGA spectra are dominated by typical PLGA peaks. Relevant to the OH stretch is the ester bond at 1754 $cm^{-1}$, the stretching vibrations of CH, CH2, and CH3 at 2884 and 3000 $cm^{-1}$, and the (C − H) bending at 846 and 1459 $cm^{-1}$, which has peaks at 3523 and 3654 $cm^{-1}$ [17, 18]. The SRF-PLGANPs IR spectra showed distinct bands that were attributed to the drug and PLGA functional groups, as shown in Fig. 2. Two out-of-plane vibrations, C-H bending vibrations, were found at 683.34 and 839.32 $cm^{-1}$. Vibrations of C-H bending were detected at 1094.05 $cm^{-1}$, C-O stretching at 1128.44 $cm^{-1}$, and C-O stretching at 925.70 $cm^{-1}$, all of which are indicative of RT vibrations at 1558.47 $cm^{-1}$.

**DSC:**

The melting endothermic peak at $199.87^0$ °C (Fig. 3) in the DSC thermogram of API demonstrated that the DSC thermograms of amorphous PLA nanoparticle (PLGA and SRF-PLGA) did not show an endothermic acute peak. One possible explanation for the lowered matching DSC thermogram of SRF-PLGANPs is the presence of an endothermic peak of SRF, which is the phase transition from crystalline to amorphous API that occurs during nan formulation. The stability of the formulation can be enhanced by nanoencapsulation, which causes amorphization and degradation of crystallinity. Both the X-ray diffraction study findings and DSC analyses were highly involved. Although the active pharmaceutical ingredient and excipient did not undergo a chemical reaction, contacts and alteration of physical appearance (crystalline-amorphous) could have been introduced during the creation of NPs, according to the temperature profiles, XRD patterns, and Fourier transform infrared spectra.

**XRD analysis**

One non-destructive and rapid analytical technique is X-ray powder diffraction (XRD), which is most often employed to study the microstructure and identify the phases in crystalline materials. This method relies on the irradiation of samples with X-rays and the determination of the scattering angle and intensity of the X-rays as they travel through the materials. The scattering angle's effect on the scattered X-rays' intensity is seen in Figure 3. Information on the placement of chemical structures can be gleaned from the scattered intensity strengths and the location of the 2θ angle. In Figure 3, we can observe the X-ray diffractograms of several substances, including physically mixed SRF, RT, and PLGA, pure PLGA, pure medicines (both SRF and RT), and SRF-PLGANPs. Sharp peaks at 2θ of 11.58 °, 18.78 °, 22.64 °, 23.08 °, 24.94 °, 25.38 °, and 38.06 °were observed in the pure-SRF diffractogram (Fig. 4), corresponding to d-values (Bragg spacing) of 7.6354, 4.7212, 3.9242, 3.8504, and 3.5673 SRF, respectively. Similar to the pure-PLGA diffractogram, this one show PLGA polymer at 1536 cps intensity and Bragg spacings of 2.3648 and 2.0456; the two sharp peaks correspond to the θ values of 38.02 °and 44.24°, respectively. It was projected that SRF-PLGANPs would show high intensities at the Bragg spacing of 2.0456 °, whereas PLGA, the pure medications (SRF and RT), would show intensities at 5.8702 °, 3.4268°, 2.3636°, and 25.98 °, respectively.

**Surface Morphology**

**AFM**

AFM was used to scan the SRF-PLGANPs particles (Figure 5). Previous research has shown that a high degree of study of AFM on dried nanoparticles is possible because of the interaction between PLGA and glass [63]. The results from the morphological analyses show that the particles are not aggregated but rather smooth, uniform, and spherical. The AFM profile heights provide information on sphericity and polydispersity. The AFM-obtained particle diameter (approximately 280 nm) differs slightly from the DLS-obtained particle diameter (approximately 160 nm) when comparing the two imaging methods. This discrepancy was confirmed by DLS measurements. While DLS measurements were performed on buffered solutions at constant temperatures, room-temperature dry air was used for AFM measurements, which allows for a wide variety of interactions (such as those with the substrate and the pliability of the nanoparticles), and hence the specified effect [64].

**SEM & TEM:**

Images acquired using a transmission electron microscope (TEM) reveal that the SRF-PLGANPs particles are uniformly round (6), with no signs of superficial fractures or abnormalities (Figure 6). The size of these particles is consistent with that of particles investigated by DLS in the past. The chosen nanoparticle formulation had a spherical surface morphology, as revealed by scanning electron microscopy (SEM). We used a scanning electron microscope to look at the SRF-PLGANPs particles' surfaces. There were round, uniform particles ranging in size from 160 to 300 nm. Using TEM, we observed the internal structure of the particles. Similar to the SEM image, the TEM investigation showed that the particle had approximately the same size and shape and a smooth surface devoid of gains, as shown in Figure. The amorphous nature of the particle was further demonstrated by the electron point image. Therefore, the created conjugate might

be utilised to transport additional drugs, contingent upon the structure and properties of the NPs.

**In-vitro Drug release assessment**

Nanoformulations can mimic in vitro the release of medications in vivo through drug release profiling. Consequently, the standard dialysis technique was used to evaluate the SRF and RT in vitro release. Both the physiological pH of 7.4 and the microenvironment-like pH of 5 in solid tumours were used to examine the release of the medicines. The concentrations of the released medications were determined using HPLC-UV. Figure 7 shows that at pH 5 and pH 7.4, the release of SRF and RT of SRF-PLGANPs was lower and the reaction time was longer. comparison to the delivery of pure medications. The NPs' slow drug release rate peaked at 48 h (SRF: 36.79 ± 2.3%) and 24 h (RT: 30.27 ± 1.9%), both at pH 5 (7). At pH 5, the pure drug release rates were maximum at 92 h, while at pH 12, they were highest at 90 h. Cumulative releases of 62.35% SRF-PLGANPs and 50.13% RT at the 240-h mark were observed at physiological pH (Fig. 8). At pH 7.4, SRF and RT also exhibited rapid launches; at 48 h, the former reached 99.78% and the latter 92.15%. Because SRF is more soluble in an acidic environment (pH 5) than in the pH environment of 7.4 expected (Park et al., 2020), the rate of release in both the pure drug formulation and the PLGA-encapsulated one was higher in a slightly acidic environment (pH 5), contrary to what would have been expected (D'Souza, 2014). Ebadi et al. (2020) found that magnetic NPs coated with PEG and PVA release SRF more rapidly at an acidic pH (4.7) than at a neutral pH.

Various kinetic models were employed to examine the rate of release of SRF and RT from SRF-PLGANPs at pH 5 and 7.4, respectively. The set included zero-order, first-order, Korsmeyer–Peppas, Hixson–Crowell, and Higuchi–Matrix models. The results indicated that PLGA-NPs, which were engineered specifically, possessed the quality of extended medication release. The two highest correlation coefficients were 0.9975 and 0.9986. The results showed that the Korsmeyer–Peppas model best represented the SRF release in SRF-PLGANPs, while the second-best model was the Higuchi–Matrix model. Accordingly, we have the following zero-order model: R2 = 0.9912 and 0.9949. At pH 5, the release of RT was best fit by the Hixson Crowell model. The zero-order model had an R2 value of 0.9974 and 0.9998, and the level of correlation was highest for the Hixson–Crowell model. when it came to describing at a pH of 7.4 and the release of RT and SRF 0.9906 and 0.9938, respectively. The fact that the two medicines showed linearity further substantiated the characteristics of SRF-PLGANPs with prolonged release in the best-fit models.

**Cell proliferation study**

Using MTT, HepG2 cells were analysed to ascertain the effects of the combination anti-cancer therapy on HCC. that had been treated with the treatment (Fig. 9). After 72 h, the cell survival of the treated cells was reduced by the pure therapies (SRF and RT), and their effects were comparable, with IC50 values of 7.69 and 8.95, respectively. In terms of lowering cancer cell viability, dual therapy (SRF-PLGANPs) proved to be far more effective than either treatment alone, regardless of the concentration range of SRF or the amount of radiation used. In the SRF-PLGANPs group, the IC50 standard was a low 0.68. The effect on the cells was similar to that of SRF-PLGANPs (IC50:0.96) after treatment with the mixture of pure drugs.

This is consistent with previous research on the carcinogenic effects of PLGA-NP cells, as demonstrated by MTT assays conducted by Elhabak et al. (2020), Mukerjee and Vishwanatha (2009), and Taebpour et al. (2). On the other hand, B-PLGA-NPs did not have a critical effect influence HepG2 cell outcomes, indicating to which the PLGA-NPs that were developed are safe to use at low concentrations without causing significant cellular cytotoxicity. When the concentration was < 3.75 µg/mL, SRF and RT had no discernible impact on cell viability; however, SRF-PLGANPs had a minor but consistent effect across the board. This suggests that HepG2 cells responded better when SRF and RT were administered together. Based on these findings, our therapeutic method has a good chance of effectively controlling HCC.

**Table 1: PLGA-NPs that were created and their physical characteristics. Deviations from the mean (mean ± SD, n = 3) are used to display the average of three measurements or more.**

| PLGA-NPs | Particle size (nm) | Polydispersity index (PDI) | Zeta potential (ζ) (mV) |
|---|---|---|---|
| SRF-PLGANPs (0.25 %, PVA) | 285.36±2.62 | 0.325±0.06 | -23.65±1.06 |
| SRF-PLGANPs (0.5 %, PVA) | 220.59±1.58 | 0.269±0.08 | -17.64±1.24 |
| SRF-PLGANP | 168.36±4.52 | 0.239±0.04 | -14.25±1.3 |

| | | | |
|---|---|---|---|
| s (1 %, PVA) | | | 5 |
| SRF-PLGANPs (1.5 %, PVA) | 296.53±3.75 | 0.351±0.02 | -20.64±1.29 |
| B-PLGANPs (1.5 %, PVA) | 146.24±2.06 | 0.175±0.09 | -18.29±1.42 |

**Table 2: The proportions of SRF-PLGANPs containing EE and DL that were prepared. (Mean + SD, n = 3) is the standard deviation of the three measurements that make up the results.**

| PLGA-NPs | %EE | | %DL | |
|---|---|---|---|---|
| | SRF | RT | SRF | RT |
| SRF-PLGANPs (0.25 %, PVA) | 79.36±3.26 | 65.34±2.36 | 6.53±0.26 | 2.56±0.35 |
| SRF-PLGANPs (0.5 %, PVA) | 80.25±2.54 | 72.34±2.41 | 7.29±0.59 | 2.95±0.61 |
| SRF-PLGANPs (1 %, PVA) | 89.36±4.15 | 79.86±3.51 | 7.65±0.75 | 3.24±0.42 |
| SRF-PLGANPs (1.5 %, PVA) | 75.43±4.27 | 68.42±2.69 | 6.86±0.14 | 3.06±0.17 |

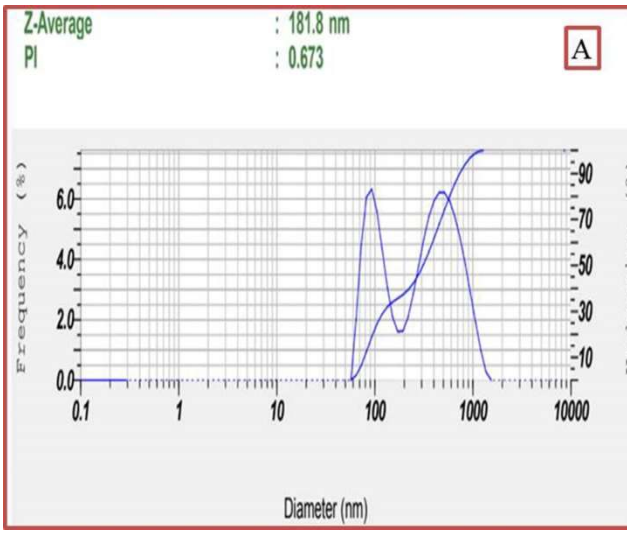


**Figure 1: A. Particle size of Optimized formulation, B. Zeta potential of optimized formulation**

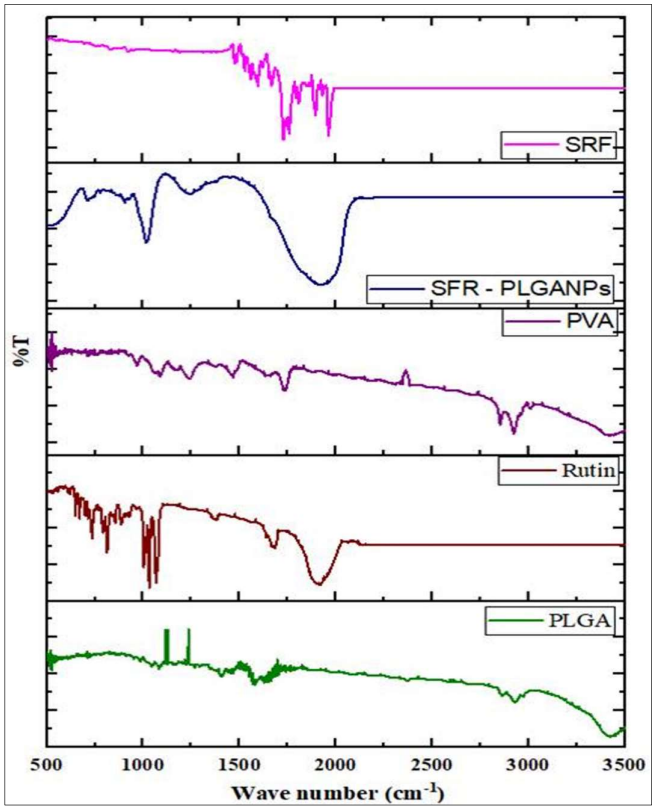


**Figure 2: This is the Fourier transform infrared spectra of the drug Rutin, PLGA, and the optimised SRF-PLGANPs formulation.**

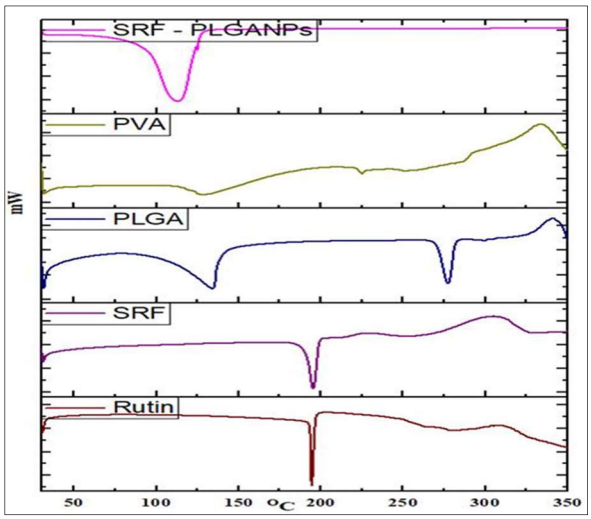


**Figure 3: Surface enthalpy scanning calorimetry (DSC) of unadulterated rutin, PLGA, and an optimised SRF-PLGANPs formulation**

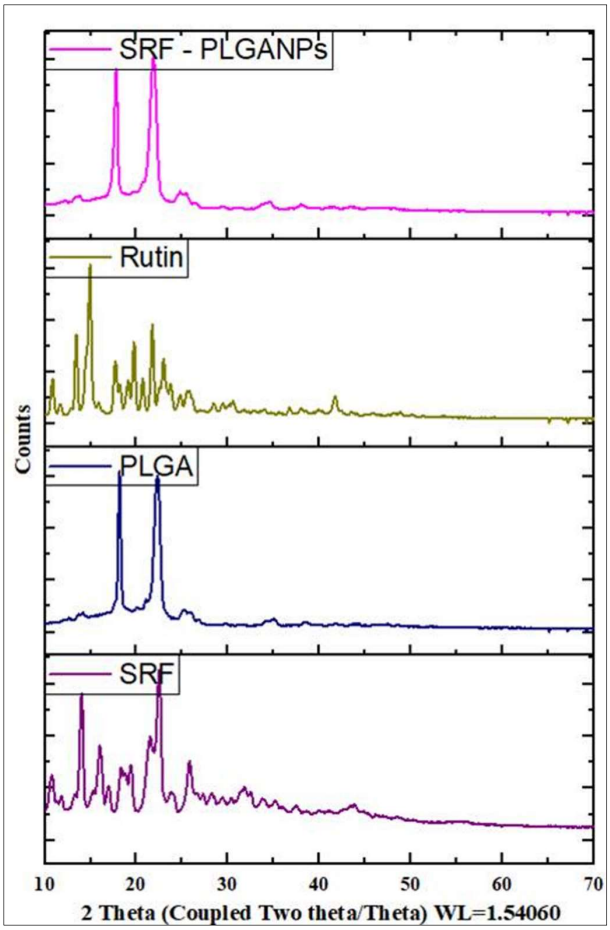


**Figure 4: Diffraction pattern of powdered X-rays from SRF-PLGANPs, Rutin, PLGA, and pure drug**

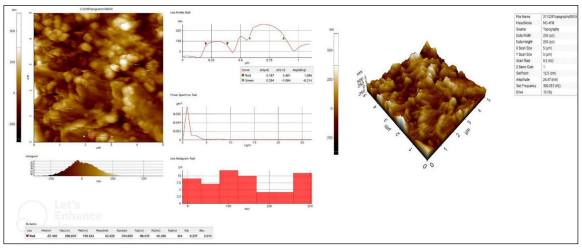

**Figure 5: 3D picture (lines of white dots in the topographical pictures) and profiles of the chosen SRF-PLGANPs particles' heights as measured by AFM in tapping mode.**

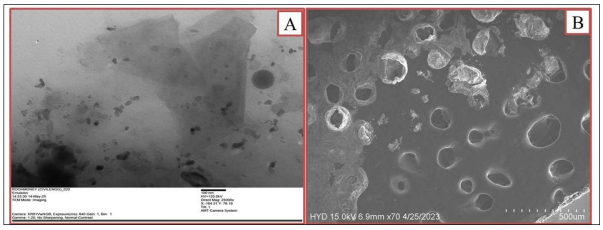


**Figure 6: The improved SRF-PLGANPs formulation was examined using scanning and transmission electron microscopy.**

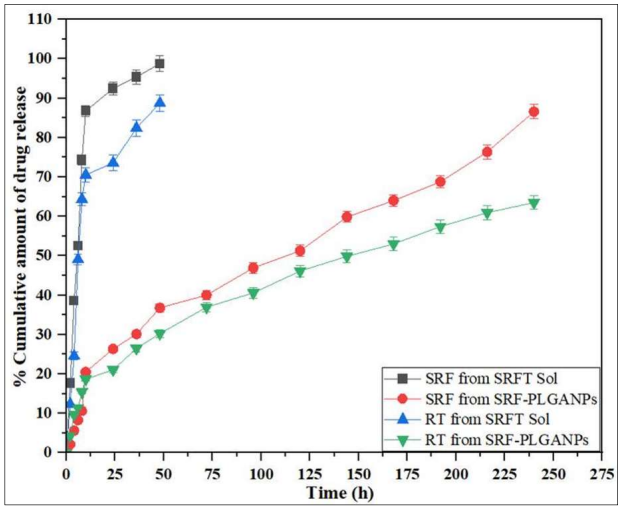


**Figure 7: Pharmacological dosage distribution of both free and bound A&R SRF medicines encased in PLGA in PBS containing 0.5% Tween-80 and kept at a pH of 5.**

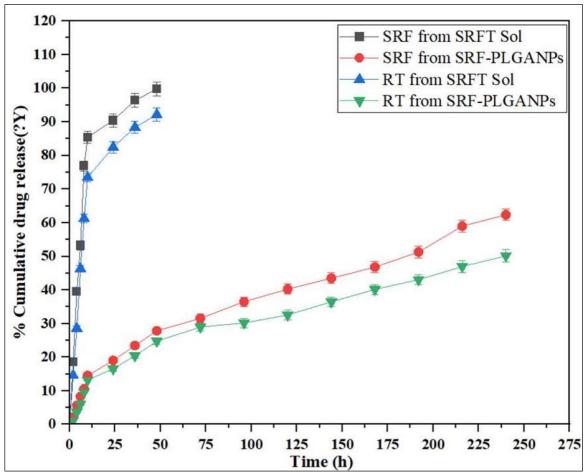


**Figure 8 shows the pharmaceutical release profile in PBS containing 0.5% Tween-80 and both the free and bound PLGA-entrapped pharmaceuticals at 7.4 SRF and room temperature. Results are shown as the average of three observations plus the standard deviation (Mean + SD, n=3), and the temperature at which the experiments were conducted was 37 +0.5 ºC.**

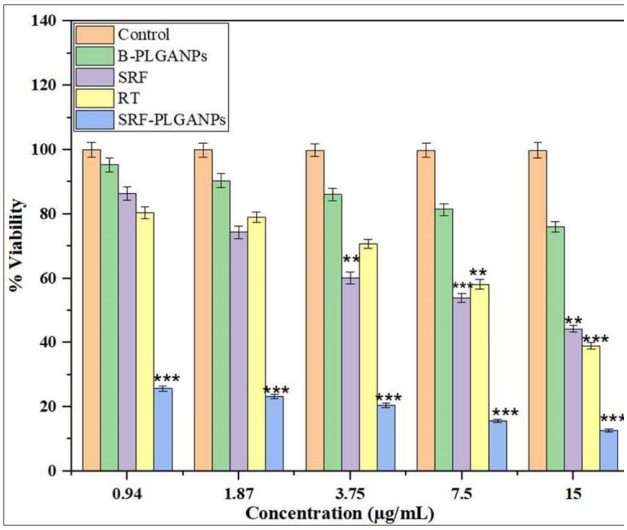


**Figure 9: Evaluation of treatment cytotoxicity on HepG2 cells using MTT assays in vitro. A full 72 hours after HepG2 cells were incubated in combination with B-PNPs and SRF, RT, or SRF-PLGANPs, the results were measured by % cellular viability as a response to the treatments. Using a standard One-way ANOVA test, we compared each group receiving therapy to a control group without any modifying factors and found statistical significance ($p < 0.01$, $p < 0.001$). Shown as the average plus standard deviation, with a sample size of 4.**

## CONCLUSION

This study used the solvent evaporation method with PLGA as a support material to manufacture sorafenib-loaded sustained-release polymeric nanoparticles. Achieving the target nano formulations with the specified encapsulation percentage (>80%), between PDI (0.239–0.04) and particle size (168.36±4.52 nm) was successful. When the nanoparticles were scanned using scanning electron microscopy, their spherical surface was revealed. The dosage form effectively encapsulated the drug, according to XRD testing. With a diameter of approximately 168 nm, a low PDI of 0.239, a low negative 0 of − 14.25 mV, and a high percentage of particle empennage (SRF: 89.36 4.15, RT: 79.86 3.51), the results demonstrated that the formulation comprised SRF-PLGANPs with 1% PVA. The nanocarriers also carried amorphous drugs, and their in vitro release patterns were unaffected by changes in pH, whether acidic or neutral. The following amounts were released after 240 h in SRF and 48 h in RT: 62.35 and 50.13 at pH 7.4 and 5, respectively. Regarding the release of the drug, kinetic models proved that the medications were released through Fickian diffusion. The cytotoxicity of the chosen formulations was examined using HepG2 cancer cell lines. Both the drug concentration and incubation duration had a significant negative impact on cell viability. These findings suggest that SRF-PLGANPs have therapeutic potential for HCC management and open new avenues for preclinical and clinical studies. Our next line of enquiry will involve studying the efficacy and safety of SRF-PLGANPs in vivo using a suitable mouse model of HCC.

## REFERENCES


1. Dimitroulis D, Damaskos C, Valsami S, Davakis S, Garmpis N, Spartalis E et al. From diagnosis to treatment of hepatocellular carcinoma: an epidemic problem for both developed and developing world. World J Gastroenterol 2017;23:5282-5294. doi:10.3748/wjg.v23.i29.5282.
2. Michielsen PP, Francque SM, Dongen, JL. Viral hepatitis and hepatocellular carcinoma. World J Surg Oncol. 2005;3:27-18.doi:10.1186/1477-7819-3-27.
3. Lin S, Hoffmann K, Schemmer P. Treatment of hepatocellular carcinoma: a systematic review. Liver cancer 2012;1,144-158.doi:10.1159/000343828.
4. Avila MA, Berasain C, Sangro B, Prieto J. New therapies for hepatocellular carcinoma. Oncogene 2006;25:3866-3884.doi:10.1038/sj.onc.1209550.
5. Surendiran A, Sandhiya S, Pradhan S, Adithan C. Novel applications of nanotechnology in medicine. Indian J Med Res. 2009;130(6):689-701.
6. Iyer R, Fetterly G, Lugade A, Thanavala Y. Sorafenib: a clinical and pharmacologic review. Expert Opin Pharmacother. 2010;11(11):1943-55doi:10.1517/14656566.2010.496453.
7. Furuse J. Sorafenib for the treatment of unresectable hepatocellular carcinoma. Biologics. 2008;2(4):779-788.doi: 10.2147/btt.s3410.
8. Laface C, Fedele P, Maselli FM, Ambrogio, F, Foti C, Molinari P, Ammendola M, Lioce M, Ranieri G. Targeted Therapy for Hepatocellular Carcinoma: Old and New Opportunities. Cancers (Basel). 2022;14(16):4028.doi:10.3390/cancers14164028 .
9. Nguyen DT, Nguyen DH, Nguyen VTH. Sorafenib as first-line treatment for patients with primary hepatocellular carcinoma: an outcome evaluation. J Int Med Res. 2023;51(6):3000605231179928.doi:10.1177/030 00605231179928.
10. Liu C, Chen Z, Chen Y, Lu J, Li Y, Wang S, Wu G, Qian F. Improving oral bioavailability of

sorafenib by optimizing the “spring” and “parachute” based on molecular interaction mechanisms. Mol Pharm. 2016;13(2):599-608.doi: 10.1021/acs.molpharmaceut.5b00837.
11. Mousa BA. Sorafenib in the treatment of advanced hepatocellular carcinoma. Saudi J Gastroenterol. 2008;14(1):40-2.doi:10.4103/1319-3767.37808.
12. Colagrande S, Inghilesi AL, Aburas S, Taliani GG, Nardi C, Marra F, Challenges of advanced hepatocellular carcinoma. World J Gastroenterol 2016;22:7645-7659.
13. Storandt M, Mahipal A, Tella SH, Kommalapati A, Jin Z. Systemic therapy in advanced Hepatocellular Carcinoma: patient selection and key considerations. J Hepatocell Carcinoma 2022;29(9):1187-1200.doi:10.2147/JHC.S365002.
14. Zhang YL, Cui XJ, Xing H, Ning HF, Dong P, Wang GZ. Molecular targeted therapy and immunotherapy in advanced hepatocellular carcinoma: a systematic review and bayesian network meta-analysis based on randomized controlled trials. Ann Med. 2023;55(2):2242384.doi:10.1080/07853890.2023.2242384.
15. Kopustinskiene DM, Jakstas V, Savickas A, Bernatoniene J. Flavonoids as anticancer agents. Nutrients. 2020;12(2):457.doi:10.3390/nu12020457.
16. Li B, Shao H, Gao L, Li H, Sheng H, Zhu L. Nano-drug co-delivery system of natural active ingredients and chemotherapy drugs for cancer treatment: a review. Drug Deliv 2022;29:2130-2161.doi:https://doi.org/10.1080/10717544.2022.2094498
17. Beecher GR. Overview of dietary flavonoids: nomenclature, occurrence and intake. J Nutr. 2003;133(10):3248S-3254S.doi: https://doi.org/10.1093/jn/133.10.3248S.
18. Yang J, Guo J, Yuan J. In vitro antioxidant properties of rutin. LWT-Food Sci Tech. 2008;41(6):1060-1066.doi: https://doi.org/10.1016/j.lwt.2007.06.010.
19. Gunathilake KDPP, Ranaweera KKDS, Rupasinghe HPV. Analysis of rutin, β-carotene, and lutein content and evaluation of antioxidant activities of six edible leaves on free radicals and reactive oxygen species, J Food Biochem. 2018;42(5):1-9.doi: https://doi.org/10.1111/JFBC.12579.
20. Lukšič L, Bonafaccia G, Timoracka M, Vollmannova A, Trček J, Nyambe TK, Melini V, Acquistucci R, Germ M, Kreft I. Rutin and quercetin transformation during preparation of buckwheat sourdough bread. J Cereal Sci. 2016;69:71-76.doi:https://doi.org/10.1016/j.jcs.2016.02.011.
21. Mauludin R, Müller RH, Keck CM. Development of an oral rutin nanocrystal formulation. Int J Pharm. 2009;370(1-2):202-9.doi:10.1016/j.ijpharm.2008.11.029.
22. Babazadeh A, Ghanbarzadeh B, Hamishehkar H. Novel nanostructured lipid carriers as a promising food grade delivery system for rutin. J Func. Foods, 2016;26:167-175.
23. Sri KV, Kondaiah A, Ratna JV, Annapurna A. Preparation and characterization of quercetin and rutin cyclodextrin inclusion complexes. Drug Dev Ind Pharm. 2007;33(3):245-53.doi:10.1080/03639040601150195.33(3):245-253.
24. Fang Z, Bhandari B. Encapsulation of polyphenols–a review. Trends Food Sci Tech. 2010;21(10):510-523.https://doi.org/10.1016/j.tifs.2010.08.003.
25. Escudero-Ortiz V, Perez-Ruixo JJ, Valenzuela B. Development and validation of an HPLC-UV method for pazopanib quantification in human plasma and application to patients with cancer in routine clinical practice. Therap Drug Monit. 2015;37(2):172-9.doi:10.1097/FTD.0000000000000121.
26. Tiwari A, Mahadik KR, Gabhe SY. Effect of piperine and its analogs on Pharmacokinetic Properties of Sorafenib Tosylate: Bioanalytical Method Development and Validation. J Appl Pharm Sci. 2020;10(12):001-012.doi:10.7324/JAPS.2020.101201.
27. Kuntić V, Pejić N, Ivković B, Vujić Z, Ilić K, Mićić S, Vukojević V. Isocratic RP-HPLC method for rutin determination in solid oral dosage forms. J pharm biomed anal. 2007;43(2):718-21.doi:10.1016/j.jpba.2006.07.019.
28. Zhou M, Zhang G, Hu J, Zhu Y, Lan H, Shen X, Lv Y, Huang L. Rutin attenuates sorafenib-induced chemoresistance and autophagy in hepatocellular carcinoma by regulating BANCR/miRNA-590-5P/OLR1 axis. Int J Biol Sci. 2021;17(13):3595-3607.doi:10.7150/ijbs.62471.
29. Kalam MA, Alshamsan A. Poly (d, l-lactide-co-glycolide) nanoparticles for sustained release of tacrolimus in rabbit eyes. Biomed Pharmacother. 2017;94:402-411.doi: 10.1016/j.biopha.2017.07.110.
30. Rezvantalab S, Drude NI, Moraveji MK, Güvener N, Koons EK, Shi Y, Lammers T, Kiessling F. PLGA-Based Nanoparticles in Cancer Treatment. Front Pharmacol. 2018;9: 1260.doi:10.3389/fphar.2018.01260.

31. Song X, Zhao Y, Wu W, Bi Y, Cai Z, Chen Q, Li Y, Hou S. PLGA nanoparticles simultaneously loaded with vincristine sulfate and verapamil hydrochloride: systematic study of particle size and drug entrapment efficiency. Int J Pharm. 2008;350(1-2):320-9. doi:10.1016/j.ijpharm.2007.08.034.
32. Yang SE, Zhang B, Gong X, Wang, T, Liu Y, Zhang N. *In vivo* biodistribution, biocompatibility, and efficacy of sorafenib-loaded lipid-based nanosuspensions evaluated experimentally in cancer. Int J Nanomed 2016;11:2329-2343.doi:10.2147/IJN.S104119.
33. Amarachinta PR, Sharma G, Samed N, Chettupalli AK, Alle M, Kim JC. Central composite design for the development of carvedilol-loaded transdermal ethosomal hydrogel for extended and enhanced anti-hypertensive effect. J Nanobiotechnol. 2021;19(1):100.doi:10.1186/s12951-021-00833-4.
34. Unnisa A, Chettupalli AK, Al Hagbani T, Khalid M, Jandrajupalli SB, Chandolu S, Hussain T. Development of Dapagliflozin Solid Lipid Nanoparticles as a Novel Carrier for Oral Delivery: Statistical Design, Optimization, *In-Vitro* and I*n-Vivo* Characterization, and Evaluation. Pharmaceuticals (Basel). 2022;15(5):568.doi: 10.3390/ph15050568.
35. Avula PR, Chettupalli AK, Chauhan V, Jadi RK. Design, formulation, *in-vitro* and in-vivo pharmacokinetic evaluation of Nicardipine-nanostructured lipid carrier for transdermal drug delivery system. Mater. today: Proceedings. Jul 2023;12.
36. Chettupalli AK, Ajmera S, Kuchukuntla M, Palanivel V, Katta S. Design Formulation of Nanospanlastic Novel Carriers as a Promising Approach to Enhanced Bioavailability in Intranasal Drug Delivery for Sinusitis: Statistical Optimization and In vitro and In vivo Characterization. Curr. Nanomed. 2024;14(3):266-88.
37. Gautam AK, Kumar P, Maity B, Routholla G, Ghosh B, Chidambaram K, Begum MY, Al Fatease A, Rajinikanth PS, Singh S, Saha S, Vijaykumar MR. Synthesis and appraisal of dalbergin-loaded PLGA nanoparticles modified with galactose against hepatocellular carcinoma: In-vitro, pharmacokinetic, and in-silico studies. Front Pharmacol. 2022;28: 13:1021867.doi:10.3389/fphar.2022.1021867. PMID: 36386226; PMCID: PMC9650263.
38. Elsewedy, H. S., Dhubiab, B. E. A., Mahdy, M. A., & Elnahas, H. M. Development, optimization, and evaluation of PEGylated brucine-loaded PLGA nanoparticles. Drug Deliv, 2020;27(1):1134-1146. https://doi.org/10.1080/10717544.2020.1797237
39. Alhudaithi SS, Kalam MA, Binobaid L, Ali R, Almutairi MM, Qamar W, Hithlayn HB, Almutairi A, Alshememry AK. Sorafenib and Piperine co-loaded PLGA nanoparticles: Development, characterization, and anti-cancer activity against hepatocellular carcinoma cell line. Saudi Pharm J. 2024;32(5):102064.
40. Alshememry AK, Kalam MA, Shahid M, Ali R, Alhudaithi SS, Alshumaimeri NA, BinHudhud ZA, Aldaham AA, Binkhathlan Z, Almomen AA. Delafloxacin-Loaded Poly(D,L-lactide-co-glycolide) Nanoparticles for Topical Ocular Use: In Vitro Characterization and Antimicrobial Activity. ACS Omega. 2024;9(5):DOI: 10.1021/acsomega.4c07805.
41. Sahdev KA, Raorane CJ, Ali MA, Mashay Al-Anazi K, Manoharan RK, Raj V, Singh A. Chitosan-Folic Acid-Coated Quercetin-Loaded PLGA Nanoparticles for Hepatic Carcinoma Treatment. Polymers (Basel). 2025;17(7):955.doi:10.3390/polym17070955. PMID:40219344:PMCID:PMC11991491.
42. Ebadi M, Buskaran K, Bullo S. Drug delivery system based on magnetic iron oxide nanoparticles coated with (polyvinyl alcohol-zinc/aluminium-layered double hydroxide-sorafenib), Alex. Eng. J. 2020;60(1):733-747. https://doi.org/10.1016/j.aej.2020.09.06.
43. Zheng N, Liu W, Li B, Nie H, Liu J, Cheng Y, Wang J, Dong H, Jia L. Co-delivery of sorafenib and metapristone encapsulated by CXCR4-targeted PLGA-PEG nanoparticles overcomes hepatocellular carcinoma resistance to sorafenib. J Exp Clin Cancer Res.2019;38:1-8.
44. Jena GK, Patra CHN, Dixit PK. Cytotoxicity and Pharmacokinetic Studies of PLGA Based Capecitabine Loaded Nanoparticles. Indian J Pharm Edu Res. 2020;54(2):349-56.
45. Bohong Guo, Danqiao Xu, Xiaohong Liu, Cancheng Liao, Shengbin Li, Zexian Huang, Xiaofang Li, Jun Yi. Characterization and cytotoxicity of PLGA nanoparticles loaded with formononetin cyclodextrin complex, Journal of Drug Delivery Science and Technology. 2017;41:375-383.doi:10.1016/j.jddst.2017.08.010.
46. Taebpour M, Arasteh F, Akhlaghi M, Haghirosadat BF, Oroojalian F, Tofighi D. Fabrication and characterization of PLGA polymeric nanoparticles containing berberine and its cytotoxicity on breast cancer cell (MCF-7). Nanomed Res J 2021;6(4):396-408. DOI:10.22034/nmrj.2021.04.009.

47. Caputo TM, Cusano AM, Principe S, Cicatiello P, Celetti G, Aliberti A, Micco A, Ruvo M, Tagliamonte M, Ragone C, Minopoli M, Carriero MV, Buonaguro L, Cusano A. Sorafenib-loaded PLGA Carriers for enhanced drug delivery and Cellular uptake in liver cancer cells. Int J Nanomedicine 2023;18:4121-4142.doi:10.2147/IJN.S415968.
48. Lu Y, Cheng D, Niu B, Wang X, Wu X, Wang A. Properties of Poly (Lactic- co-Glycolic Acid) and Progress of Poly (Lactic-co-Glycolic Acid)-Based Biodegradable Materials in Biomedical Research.Pharmaceuticals (Basel).2023;16(3):454.doi:10.3390/ph16030454.
49. Rocha CV, Goncalves V, da Silva MC, Banobre-Lopez M, Gallo J. PLGA- based composites for various biomedical applications. Int J Mol Sci. 2022;23(4):2034.doi: 10.3390/ijms23042034.